

Chemical Targeting of Rhodol Voltage Sensitive Dyes to Dopaminergic Neurons

Tomas Fiala, Eugene V. Mosharov, Jihang Wang, Adriana M. Mendieta, Se Joon Choi, Eva Fialova, Christopher Hwu, David Sulzer* and Dalibor Sames*

KEYWORDS: *voltage sensitive dyes, chemical targeting, cell-type specific imaging, molecular imaging probes.*

ABSTRACT: Optical imaging of changes in membrane potential of living cells can be achieved by the means of fluorescent voltage sensitive dyes (VSDs). A particularly challenging task is to efficiently deliver these highly lipophilic probes to specific neuronal subpopulations in brain tissue. We have tackled this task by designing a solubilizing, hydrophilic polymer platform that carries a high-affinity ligand for a membrane protein marker of interest and a fluorescent VSD. Here, we disclose an improved design of polymer supported probes for chemical, non-genetic targeting of voltage sensors to axons natively expressing the dopamine transporter in *ex vivo* mouse brain tissue. We first show that for negatively charged rhodol VSDs functioning on the photoinduced electron transfer principle, poly(ethylene glycol) (PEG) as a carrier enables targeting with higher selectivity than the polysaccharide dextran in HEK cell culture. In the same experimental setting, we also demonstrate that incorporation of an azetidine ring in the rhodol chromophore substantially increases the brightness and voltage sensitivity of the respective VSD. We show that the superior properties of the optimized sensor are transferable to recording of electrically evoked activity from dopaminergic axons in mouse striatal slices after averaging of multiple trials. Finally, we suggest the next milestones for the field to achieve single-scan recordings with non-genetically targeted VSDs in native brain tissue.

Introduction

Recording the electrical transients that accompany signal transduction within neuronal cells is a key tool in experimental neuroscience but remains a great challenge. The standard method for recording changes in membrane potential relies on whole cell electrophysiology, which is, however, invasive and low throughput.^{1,2} More recently, optical methods to interrogate signal transduction in neurons have emerged as a viable alternative to patch-clamp techniques.^{3,4} Visualizing calcium transients with fluorescent calcium sensitive dyes, both synthetic⁵⁻⁸ and protein-based,⁹⁻¹¹ have become a highly popular optical approach to indirectly interrogate neuronal activity. Neurotransmitter release, the result of a depolarization cascade, has been optically visualized by chemical tracers (fluorescent false neurotransmitters, FFNs),¹²⁻¹⁹ chemical sensors²⁰⁻²³ or genetically encoded sensors.²⁴

A great deal of effort has also been invested in direct optical readout of membrane potential changes with voltage sensitive dyes (VSDs).²⁵⁻²⁸ Synthetic voltage sensors based on various mechanisms have been developed,²⁶ some examples of which include electrochromic,²⁹⁻³¹ semiconductor nanoparticle-based,^{32,33} redistribution-based³⁴ or photoinduced electron transfer (PeT)-based sensors.³⁵⁻⁴⁵ A major shortcoming of synthetic VSDs has been their lack of selectivity for specific neuronal subpopulations. This challenge has been partially tackled by genetically-encoded voltage indicators (GEVIs) – protein-based sensors which optically respond to changes in membrane potential and

can be expressed in defined cells via cell-type specific promoters.^{46,47} Small-molecule dyes, however, have several advantages over protein-based probes, including the availability of a broad palette of structural features for tuning the photophysical properties of the probe.^{48,49} Hybrid chemo-genetic approaches have successfully fused the advantages of synthetic dyes with those of genetic targeting, either by conjugating voltage sensitive domains with small-molecule fluorophores,⁵⁰⁻⁵³ or by enzymatically decaging⁵⁴⁻⁵⁷ or anchoring⁵⁸⁻⁶¹ synthetic VSDs. Targeted delivery of synthetic VSDs, however, remains a challenge due to the high lipophilicity of these sensors, resulting in background staining.

All targeting approaches mentioned above require genetic alteration of the brain tissue in the species of interest. We wondered whether targeted voltage imaging could be achieved by a purely chemical approach. We recently disclosed VoLDeMo (Voltage sensor–ligand–dextran targeted to monoaminergic neurons) as the first example of a VSD targeted to specific neuronal subpopulations without the use of genetic manipulation.⁶² In our design, we used dichloropane, a tropane analog, as a targeting ligand with high affinity for monoamine transporters.^{63,64} As a carrier, we used the polysaccharide dextran which compensates for the hydrophobic properties of the VSD and functions as a molecular platform supporting both the sensor as well as the targeting ligand. The design using the dextran polymer carrier proved to be universal, as both positively charged, electrochromic aminonaphthyl-ethylene-pyridinium

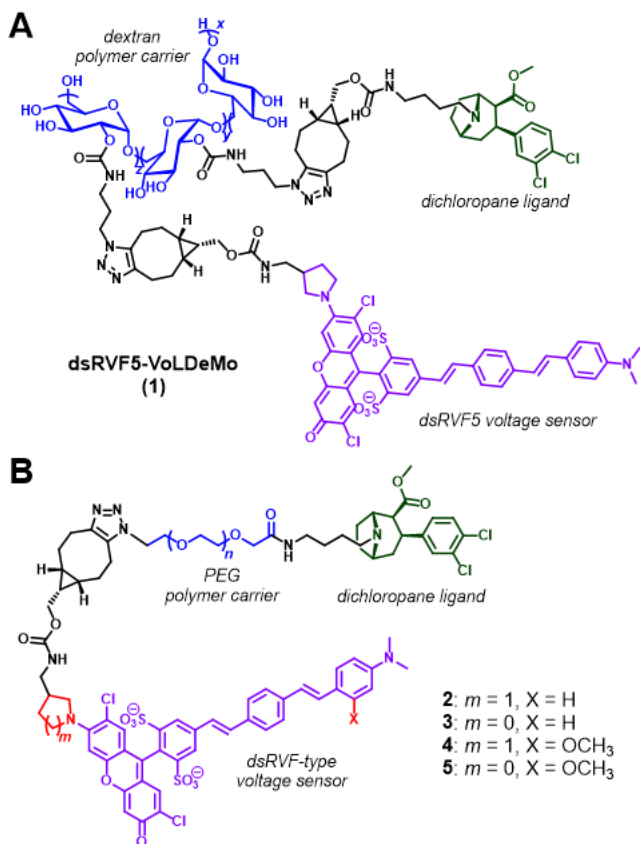


Figure 1. Structures of polymer supported, non-genetically targetable VSDs. (A) *Previous work*: the dextran-supported dsRVF5-VoLDeMo probe (**1**).⁶² (B) *This work*: a series of PEG supported VSDs (**2–5**). Variations of structural features of the original dsRVF5 VSD are highlighted in red.

(ANEP)-type VSDs and negatively charged, PeT-based VSDs were successfully targeted by this approach. Our lead prototype probe, dsRVF5-VoLDeMo (**1**; Figure 1A) enabled selective voltage recording from dopaminergic axons in brain tissue. The use of dextran as the polymer carrier, however, posed a significant disadvantage – the chemistry to functionalize the polysaccharide is not trivial and a distribution of functionalized species is always obtained.

Poly(ethylene glycol) (PEG) has been widely used as a platform for well-defined bifunctional sensors^{58–61,65} or drugs,^{66–70} combining the advantages of easy synthesis from commercial heterobifunctional precursors and favorable physico-chemical properties, such as high water solubility and low protein binding.⁷¹ Several hybrid chemogenetically targeted voltage sensors based on a PEG carrier have been developed.^{58–61} We therefore sought to systematically compare the dextran and PEG platforms in the context of our purely chemical, non-genetic targeting.

In this work, we show that although dextran is a more universal carrier for targetable VSDs, PEG-supported negatively charged rhodol VSDs (Figure 1B) are superior in terms of targeting selectivity. We use the new design to prepare improved, brighter and more voltage sensitive targeted VSDs by incorporating azetidines substituents in the chromophore core. We show that the new generation of targeted VSDs retains excellent selectivity for dopaminergic axons in mouse striatal slices and can be used for

recording electrically evoked activity in this system after signal averaging.

Results and Discussion

Design of PEG-supported targeted rhodol VSDs. From the original design of our dextran-based dsRVF5-VoLDeMo probe (**1**, Figure 1A), we first retained both the dichloropane ligand as the targeting entity and the dsRVF5 VSD, a disulfonated (ds)³⁸ rhodol voltage fluor (RVF)³⁹ containing a five-membered (5) pyrrolidine ring. Instead of the polysaccharide dextran, we used a linear PEG carrier with an average M_w of 3500 Da ($n \sim 80$) based on the following considerations: the length of this linker is ~ 29 nm (calculated based on ref.⁵⁹), which we hypothesized would suffice to enable insertion of the dichloropane ligand into the membrane-spanning dopamine transporter (DAT) protein,⁷² allow insertion of the VSD into the cell membrane (which is ~ 4 nm thick²⁶) and provide sufficient additional flexibility to the polymer carrier. We prepared the dsRVF5-PEG(3500)-dichloropane probe (**2**, Figure 1B) by a simple, two-step synthesis from the commercially available N_3 -PEG(3500)-COOSu (Su = succinimidyl), via amidation with an aminobutyl derivative of dichloropane and subsequent attachment of a bicyclo[6.1.0]nonyne (BCN)-functionalized dsRVF5 by strain-promoted azide-alkyne cycloaddition (Supporting information).

Next, we varied two structural parameters of the VSD, aiming to produce targetable sensors with superior sensitivity than those carrying dsRVF5. Azetidinesubstitution has been introduced as a general strategy to improve the brightness of organic fluorophores.⁷³ Up to four-fold increase in brightness of rhodol fluorophores was reported with azetidinesubstitution compared to unstrained amine substitution.⁷³ We hypothesized that such a sizable increase in brightness would significantly increase the signal-to-noise ratio (SNR) of membrane potential recordings, since the SNR scales with the square root of brightness.⁵⁹ We therefore synthesized dsRVF4-PEG(3500)-dichloropane (**3**, Figure 1B) which, to the best of our knowledge, is the first example of an azetidinesubstituted PeT-based VSD. As the second structural modification, we introduced a methoxy substituent to the π -wire of RVF5, obtaining dsRVF5(OMe)-PEG(3500)-dichloropane (**4**, Figure 1B). A methoxy group in this position of PeT-based VSDs was reported to increase their $\Delta F/F$ voltage sensitivity (which scales linearly with the SNR⁵⁹) by increasing the probability of electron transfer.³⁶ Since the increased PeT probability results in reduced brightness of the chromophore, we also synthesized dsRVF4(OMe)-PEG(3500)-dichloropane (**5**, Figure 1B), a probe with both structural modifications combined. In this probe, we aimed to compensate for the loss in brightness from the methoxy substitution with the brightness-boosting azetidinesubstitution.

Targeting selectivity comparison of dextran- and PEG-supported dsRVF5 probes. To commence our investigations of the targeting properties of the dextran- vs. PEG-supported probes (**1** and **2**, respectively), we first compared the potency of the probes to block hDAT, a proxy of the probes' binding strength to the transporter. Probe **2** inhibited the uptake of APP+ (a fluorescent DAT substrate⁷⁴) by HEK-293 cells stably transfected with human DAT (hDAT-HEK cells) with an IC_{50} of (19 ± 2) nM

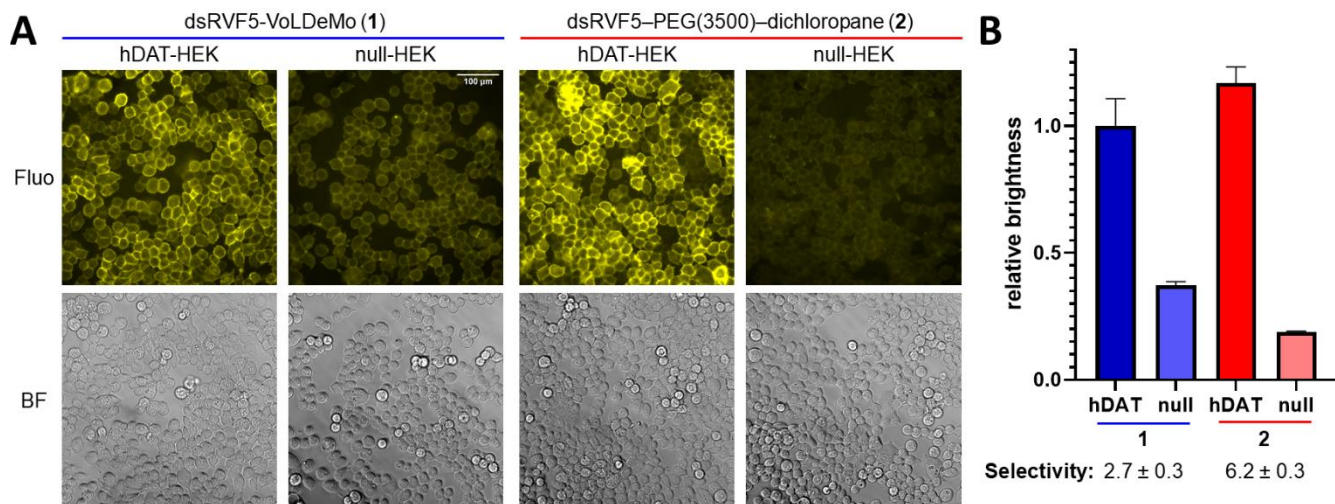


Figure 2. Comparison of the targeting selectivity of the dextran-supported probe **1** and the PEG-supported probe **2** in HEK cell culture. (A) Representative fluorescence (Fluo, *top row*) and the corresponding brightfield (BF, *bottom row*) microscopy images of HEK cells labeled with **1** (100 nM VSD, 15 min) or **2** (100 nM, 15 min). Labeling was compared in hDAT-HEK cells (*left column in each pair*) and null-HEK cells (*right column in each pair*). All fluorescence microscopy images were equally contrasted. Excitation filter: 540 nm (25 nm bandpass), 570 nm dichroic, emission filter: 605 nm (55 nm bandpass). (B) Mean fluorescence intensity of randomly selected cell bodies ($n = 3$, 5 ROIs per n) stained with probes **1** (blue) and **2** (red) as described in panel (A), normalized to the mean of probe **1**, hDAT condition (left panel in A). Error bars are \pm SEM for $n = 3$ experiments, 5 cells per n .

(Figure S1). The potency of PEG-supported probe **2** was higher than what we determined for the dextran-supported probe **1** under identical conditions: $IC_{50} = (45 \pm 2)$ nM.⁶² We hypothesize, that the more flexible PEG linker allows for better accommodation of the dichloropane ligand in the deep pocket of DAT resulting in increased binding potency.

Based on these data, we proceeded with directly comparing the targeting selectivity of probes **1** and **2** at a concentration at which both probes saturate the target protein. We labeled hDAT-HEK cells and HEK cells transfected with an empty vector (null-HEK cells) with probes **1** and **2** (100 nM VSD, 15 min) and compared the labeling patterns via one-photon excitation fluorescence microscopy (Figure 2A). For both probes, a clear membrane-localized fluorescent labeling pattern was observed in hDAT-HEK cells, which was greatly diminished in the control null-HEK cell line. Notably, the labeling selectivity of the PEG-supported probe **2** (6.2 ± 0.3 fold, $n = 3$, $P = 0.0043$, two-tailed unpaired t-test; Figure 2B) was significantly greater ($P = 0.017$, two-tailed unpaired t-test) than that of dextran-supported probe **1** (2.7 ± 0.3 fold, $n = 3$, $P = 0.026$, two-tailed unpaired t-test; Figure 2B) under the same labeling conditions. These results demonstrate that for negatively charged RVF-type VSDs, PEG is a superior polymer carrier compared to dextran in the context of targeting selectivity. We hypothesize that the observed improvement can be attributed to the lower propensity of PEG to non-specific binding to biomolecules on the cell surface compared to dextran.⁷⁵

Characterization of the targeting and brightness of PEG-supported probes carrying modified rhodol VSDs. With the superior properties of PEG as a carrier for the dsRVF5 VSD established, we proceeded with evaluating probes **3–5** carrying modified sensors compared to probe **2** (Figure 3A). We first verified that alteration of VSD struc-

ture by azetidine substitution at the chromophore or methoxy substitution at the π -wire do not affect the binding of the probe to hDAT. Probe **5**, as a representative carrying both structural modifications, blocked hDAT with an IC_{50} of (14 ± 1) nM (Figure S2), similar to that found for probe **2** [$IC_{50} = (19 \pm 2)$ nM, *vide supra*]. The structural alterations of the VSD therefore had only a negligible effect on the probe affinity to hDAT.

We next quantitatively evaluated the relative brightness of the PEG-supported probes **2, 3, 4** and **5** in labeled cells to determine the effects of pyrrolidine vs. azetidine ring and methoxylation of the π -wire on this crucial parameter (Table 1, Figure 3A, B). All four probes had very similar excitation and emission profiles when targeted to hDAT-HEK cells with only a minor hypsochromic shift observed in the azetidine-ring-containing probes **3** and **5** (Table 1, Figure S3). This fact warranted the use of a single set of excitation and emission filters for evaluating their relative cellular brightness (540/25 nm excitation filter, 605/55 nm emission filter). As expected, changing the pyrrolidine ring in dsRVF5-containing probe **2** for an azetidine ring in dsRVF4-containing probe **3** led to a 2.9-fold increase in brightness in hDAT-HEK cells labeled with the probes (50 nM, 15 min). The opposite effect was observed upon addition of a methoxy group to the phenylene-vinylene π -wire – dsRVF5(OMe) probe **4** had only 0.26 \times the brightness of the parent dsRVF5 probe **2**. Unfortunately, the azetidine ring did not fully compensate for the brightness loss caused by the π -wire methoxy group in dsRVF4(OMe) probe **5**, which had only 0.39 \times the brightness of the parent dsRVF5-containing probe **2**, or 1.5 \times the brightness of dsRVF5(OMe) probe **4**.

We also characterized the derivatized probes **3, 4** and **5** in comparison to the dsRVF5 probe **2** in terms of targeting selectivity in HEK cells. The higher affinity of the PEG-supported probes towards hDAT warranted the use of

Table 1. Targeting selectivity and brightness of dsRVF-PEG-dichloropane probes.

probe	VSD	exc. max. ^a (nm)	em. max. ^a (nm)	relative brightness ^{b,c}	selectivity ^{c,d} (hDAT/null)
2	dsRVF5	554	578	1.0 ± 0.1	6.2 ± 0.8
3	dsRVF4	548	574	2.9 ± 0.2	4.2 ± 0.4
4	dsRVF5(OMe)	555	577	0.26 ± 0.03	10 ± 1
5	dsRVF4(OMe)	549	571	0.39 ± 0.05	9 ± 1

^aExcitation at 590 nm emission. Emission at 530 nm excitation. Measured in hDAT-HEK cells labeled with the respective probe (250 nM, 15 min).

^bData collected in hDAT-HEK cells labeled with the respective probe (50 nM, 15 min). ^cExcitation filter: 540 nm (25 nm bandpass), 570 nm dichroic, emission filter: 605 nm (55 nm bandpass). Values represent mean ± SD from $n = 6$ experiments, 5 ROIs per n . These data were analyzed by an evaluator blinded to the probe and cell type. ^dRatio of the labeling intensities (after background subtraction) of hDAT-HEK cells and null-HEK cells labeled with the respective probe (50 nM, 15 min).

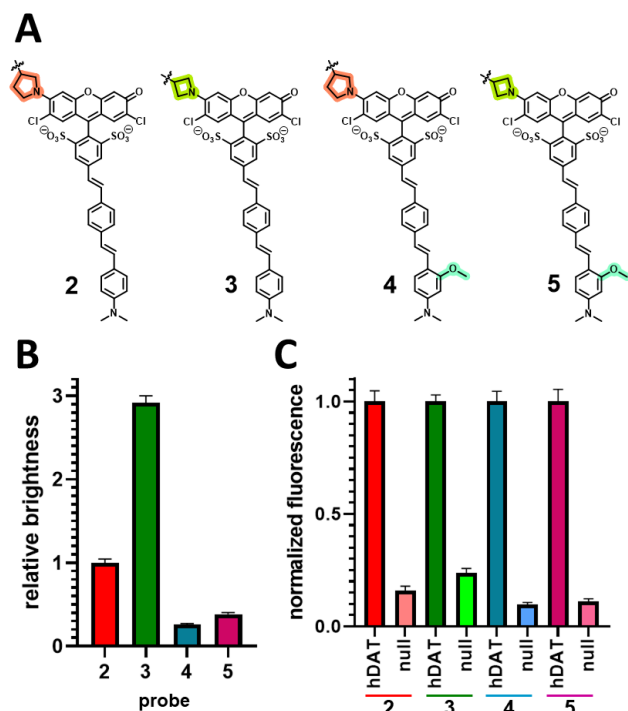


Figure 3. (A) Structures of the VSD units in probes 2, 3, 4 and 5 with highlighted structural differences: pyrrolidine (red) vs. azetidine (green) substitution on the rhodol chromophore; and methoxylation of the π -wire (teal). (B, C) Relative brightness and targeting selectivity of PEG-supported probes. hDAT-HEK cells and null-HEK cells were labeled with probes 2, 3, 4 or 5 (50 nM, 15 min). Images were taken with one-photon excitation fluorescence microscopy. Excitation filter: 540 nm (25 nm bandpass), 570 nm dichroic, emission filter: 605 nm (55 nm bandpass). All graphs represent mean \pm SEM of randomly selected cell bodies for $n = 6$ experiments, 5 ROIs per n . Analysis was carried out by an evaluator blinded to the probe and cell type. (B) Relative brightness of probes 2, 3, 4 and 5. Comparison of the mean fluorescence intensity of hDAT-HEK cells labeled with each probe, normalized to the parent dsRVF5 probe 2. (C) Targeting selectivity of probes 2, 3, 4 and 5. Comparison of the mean fluorescence intensity of hDAT- and null-HEK cells labeled with the respective probe, normalized to the hDAT condition for each probe.

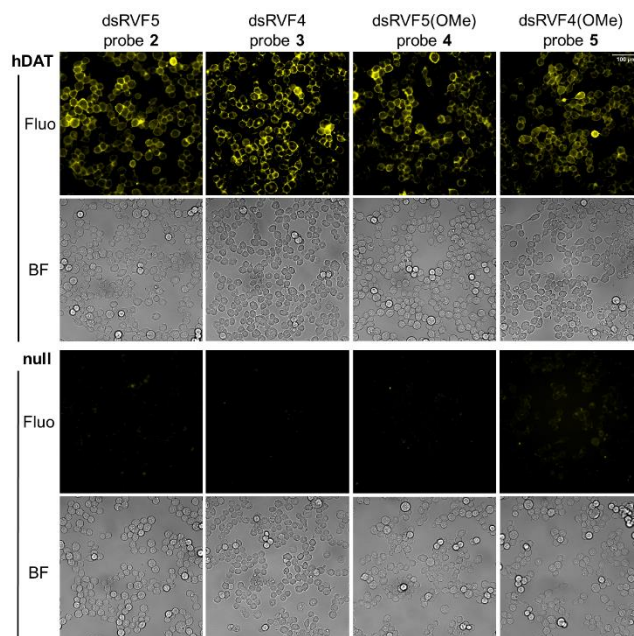


Figure 4. Characterization of the targeting of dextran-supported probes in HEK cell culture. Representative fluorescence (Fluo, top row in each pair) and the corresponding brightfield (BF, bottom row in each pair) microscopy images of HEK cells labeled with probes 2, 3, 4 and 5 (50 nM, 15 min). Labeling was compared in hDAT-HEK cells (hDAT, top two rows) and null-HEK cells (null, bottom two rows). Fluorescence microscopy images in the same column were equally contrasted. Excitation filter: 540 nm (25 nm bandpass), 570 nm dichroic, emission filter: 605 nm (55 nm bandpass).

lower concentrations than with dextran-supported probe 1. Incubating hDAT-HEK cells with either of the probes 2, 3, 4 and 5 (50 nM, 15 min) provided membrane localized fluorescence which was largely diminished in null-HEK cells ($P < 0.0001$ for all probes, $n = 6$, two-tailed unpaired t-test; Table 1, Figure 3C, Figure 4). The labeling selectivity ranged from 4.2 \pm 0.4 for dsRVF4 probe 3 to 10 \pm 1 for dsRVF5(OMe) probe 4 (Table 1, Figure 3C). The trend in labeling selectivity inversely follows that of the relative brightness of the probes, *i.e.*, the brightest probe 3 exhibits the lowest selectivity. We thus hypothesize that the apparent higher selectivity for the probes with low brightness is caused by the fact that their non-specific staining of null-HEK cells produces a signal barely above the background.

Voltage sensitivity in HEK cells. The next question we asked was how the voltage sensitivity of the PEG-supported probes **2**, **3**, **4** and **5** compares to that of the dextran-supported probe **1**. We carried out voltage clamp experiments on hDAT-HEK cells labeled with each of the probes (100 nM, 60 min). Using the patch-clamp technique, the cells were clamped at a -60 mV potential to mimic the typical resting potential of a living cell. Then, the potential was altered to hyper- and depolarizing values ranging from -100 mV to $+90$ mV and simultaneously imaged on an epifluorescence microscope. Two images at each voltage were acquired at 20 Hz (a representative trace corresponding to probe **3** is shown in Figure 5A). Plotting the fractional fluorescence change against the membrane potential provided a linear dependence for all probes (Figure 5B). The slope of this linear dependence, $\Delta F/F$ per 100 mV (Figure 5C, Table 2), together with the signal-to-noise ratio (SNR; Figure 5D, Table 2) provided comparative measures of the voltage sensitivity of the probes. We note that for the methoxylated dsRVF5-containing probe **4**, measurements at 100 nM provided poor signal due to its low brightness, which did not allow accurate determination of $\Delta F/F$ per 100 mV at this concentration. Therefore, 200 nM was used for probe **4**.

Comparing the performance of dextran-supported probe **1** ($15.1 \pm 1.0\%$, SNR = 5.2, $n = 18$) and the PEG-supported probe **2** carrying the same dsRVF5 VSD ($10.9 \pm 0.9\%$, SNR = 3.0, $n = 15$), the voltage sensitivity was significantly reduced ($P = 0.0049$, two-tailed unpaired t -test) in the case of the PEG-supported probe (Figure 5C, D, Table 2). We hypothesize that this reduction in sensitivity may be caused by less optimal orientation of the VSD within the cell membrane in probe **2** with the long PEG linker. The importance of the correct orientation of PeT-based VSDs in the cell membrane is known.³⁸ Dependence of voltage sensitivity on the linker length has been previously observed in chemo-genetically targeted VSDs.⁶⁰ Optimization of the PEG linker length may be necessary to minimize the loss of voltage sensitivity of the PEG-supported probe compared to the ones with a dextran carrier.

Probes **3**, **4** and **5** carrying modified variants of the dsRVF-type VSD exhibited improved voltage sensitivity, all in the range of 16.7–18.0% $\Delta F/F$ per 100 mV compared to PEG-supported dsRVF5 probe **2** ($P < 0.0001$, two-tailed unpaired t -test; Figure 5C, Table 2). Despite the similar $\Delta F/F$ per 100 mV for probes **3**–**5**, probe **3** containing the brightest, azetidine substituted and non-methoxylated dsRVF4 VSD provided voltage-dependent fluorescence with the highest SNR of 7.8, a 2.6-fold increase compared to the less bright reference dsRVF5-containing probe **2**

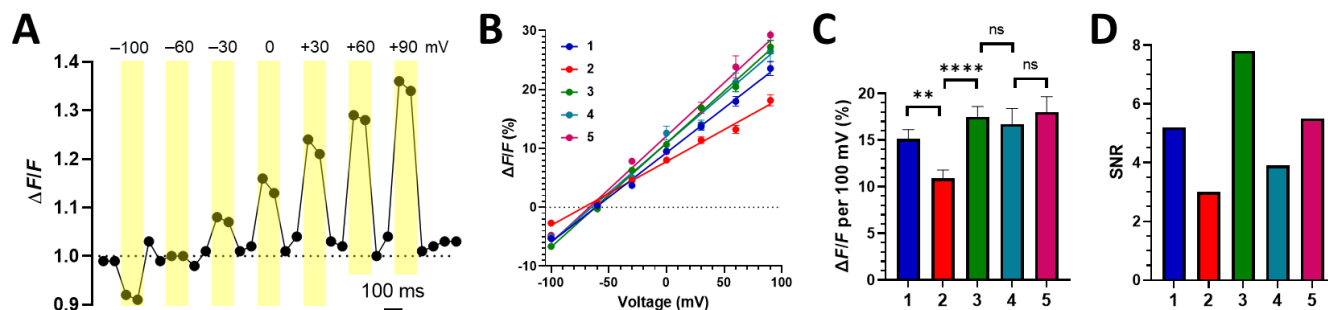


Figure 5. Membrane potential sensitivity of dextran- and PEG-supported probes in hDAT-HEK cells. (A) Representative trace of the fractional change in fluorescence of probe **3** (100 nM, 60 min) versus time of a voltage-clamped hDAT-HEK cell held at -60 mV and then subjected to 100 ms voltage holdings ranging from -100 mV to $+90$ mV. Images were taken with one-photon excitation fluorescence microscopy. Excitation filter: 545 nm (30 nm bandpass), 570 nm dichroic, emission filter: 620 nm (60 nm bandpass). (B) Plot of percent fluorescence change of probes **1**–**5** versus membrane voltage under the conditions from panel A. Individual data points represent the mean \pm SD for $n = 11$ – 18 . (C) Bar graph summarizing the slope of the linear dependence shown in panel B ($\Delta F/F$ per 100 mV) for each probe (mean \pm SEM). Two-tailed unpaired t -test, ****: $P < 0.0001$, **: $P < 0.01$, ns: $P > 0.05$ (not significant). (D) Bar graph summarizing the SNR of the voltage response for each probe calculated as $(\Delta F/F \text{ per } 100 \text{ mV})/\text{SD}$ of the background. *Note:* the concentration used for probe **4** was 200 nM, unlike for all the other probes where 100 nM was used.

Table 2. Voltage sensitivity of dextran- and PEG-supported targetable VSDs.

probe	carrier	VSD	$\Delta F/F$ per 100 mV ^a (%)	SNR ^b
1	dextran	dsRVF5	15.1 ± 1.0	5.2
2	PEG	dsRVF5	10.9 ± 0.9	3.0
3	PEG	dsRVF4	17.5 ± 1.1	7.8
4	PEG	dsRVF5(OMe)	16.7 ± 1.7^c	3.9 ^c
5	PEG	dsRVF4(OMe)	18.0 ± 1.7	5.5

^aSlope of the linear dependence of fluorescence of hDAT-HEK cells labeled with the respective probe (100 nM, 60 min) on membrane voltage under the conditions as described in Figure 5 (mean \pm SEM). ^bSignal-to-noise ratio (SNR) of the voltage response for each probe under the conditions described in Figure 5 calculated as $(\Delta F/F \text{ per } 100 \text{ mV})/\text{SD}$ of the background. ^cConcentration of 200 nM was used.

(SNR = 3.0). Also probe 5 (SNR = 5.5), containing both π -wire methoxylation and azetidine-substitution of the xanthene core [dsRVF4(OMe)], proved superior to the dsRVF5(OMe)-containing probe 4 (SNR = 3.9), highlighting the importance of increased brightness originating from the azetidine-substituted chromophore. Nevertheless, the effective sensitivity of probe 5 remained lower than that of probe 3, which lacks a methoxy substituent on the π -wire. Overall, these results show that azetidine substitution of the xanthene core in PeT-based VSDs is a promising strategy to design probes with enhanced sensitivity and brightness.

Targeting and voltage sensitivity in acute mouse brain slices. With the improved targeting selectivity and voltage sensitivity of the new PEG-supported VSDs established in cultured cells overexpressing the target DAT protein, we aimed to explore the performance of the probes *ex vivo* in acutely prepared mouse brain slices. This environment poses a great challenge for targeting lipophilic sensors due to the relatively low, native expression

levels of protein targets on the neuronal cells of interest and an abundance of “competing” non-target cells and extracellular matrix which lack the protein target. We first determined the labeling selectivity of probes 2, 3 and 5 (leaving out probe 4 which did not exhibit sufficient brightness). To compare the performance of the probes with the previously established dextran-supported probe 1 (ref.⁶²), we focused on the dorsal striatum (dSTR), a region rich in arborized dopaminergic axonal projections expressing DAT originating in substantia nigra compacta (SNc, Figure 6A). Mouse striatal slices incubated with either of the probes 2, 3 or 5 (100 nM, 30 min) exhibited a dense string-like labeling pattern as shown by two-photon excitation fluorescence microscopy (Figure 6B, C, Figure S4A), consistent with the highly arborized dopaminergic axons in this region and comparable to the pattern observed for dextran-supported probe 1 under the same conditions.⁶² As a negative control, we carried out the labeling using probe 5 in the presence of the DAT blocker nomifensine (2 μ M). A contrasting pattern of only weak,

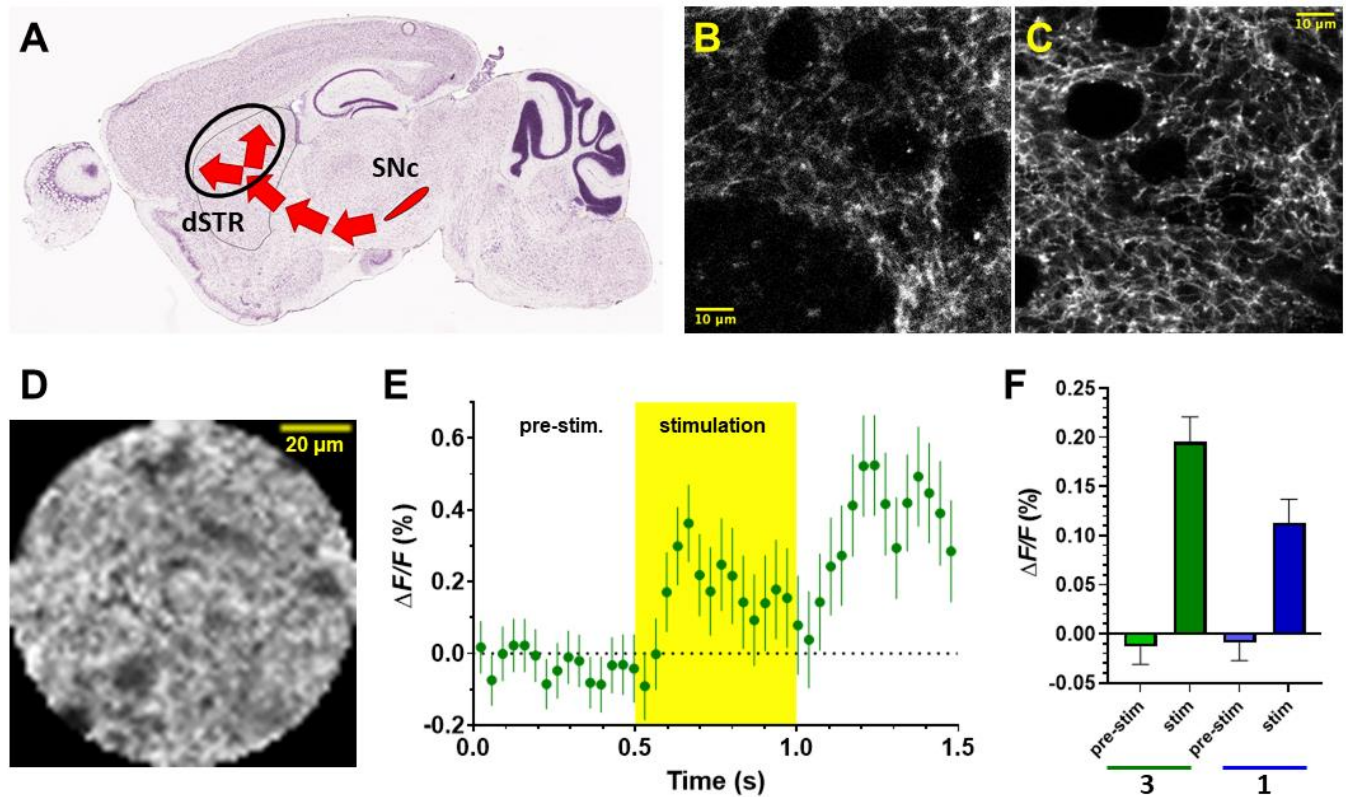


Figure 6. Targeting and voltage imaging with dextran supported probes in mouse striatal slices. (A) Nissl stained sagittal slice of a mouse brain (image credit: Allen Institute^{76,77}) with the red arrows schematically representing the placement of dopaminergic axons originating in the SNc and arborizing in the dSTR. The black oval indicates the approximate region where the images in panels B, C and D were acquired. (B, C) Representative images of mouse striatal slices labeled with probes 2 (panel B) and 3 (panel C) (100 nM, 30 min, 15 μ m depth from the tissue surface). Excitation: 820 nm, emission: 570–610 nm. (D) Representative image of a single two-photon spiral scan frame (35 μ m depth from the tissue surface) from the recording of evoked activity in panel E, demonstrating the field of view and spatial resolution. (E) Fluorescence trace recorded at 30 Hz from striatal slices labeled with probe 3 (500 nM, 30 min) with electric stimulation (25 pulses at 50 Hz, period highlighted in yellow). The trace is normalized to an analogous experiment conducted in the presence of TTX (1 μ M) and is an average from multiple trials ($n = 100$ from 10 slices). A two-point moving average was applied to smoothen the trace. (F) Mean fluorescence (\pm SEM) of voltage recording from (E) during the stimulation and pre-stimulation periods, compared to an analogous experiment with the dextran-supported probe 1 (taken from ref.⁶²). Probe 3 exhibits a $\Delta F/F$ of $0.20 \pm 0.03\%$ ($n = 100$ from 10 slices, $P < 0.0001$, two-tailed unpaired t -test), which is a 67% increase in sensitivity compared to probe 1 exhibiting a $\Delta F/F$ of $0.12 \pm 0.03\%$ ($n = 100$ from 10 slices).⁶²

diffuse background staining was observed in this case (Figure S4B, C) showing the excellent targeting selectivity of this class of probes to DAT in the complex environment of *ex vivo* brain tissue.

Given our previous experience with voltage recordings of electrically evoked activity using the dextran-supported dsRVF5 probe **1** in striatal slices, we decided to compare its performance to that of the optimized, brighter probe **3**. Specifically, we labeled striatal slices with probe **3** (500 nM, 30 min) and placed a bipolar electrode to the vicinity of a region of interest (ROI). Then, we recorded two-photon excitation fluorescence images with spiral scanning at 30 Hz for 3.5 s (Figure 6D), while stimulating the slice with the bipolar electrode delivering 25 pulses at 50 Hz from $t = 0.5$ to 1.0 s. To control for any voltage-independent artifacts during the stimulation process, we conducted the same experiment in the presence of 1 μ M tetrodotoxin (TTX). Raw traces from multiple trials ($n = 100$ from 10 slices) were corrected for photobleaching and averaged. The trace recorded in the presence of TTX was subtracted (as the voltage-independent baseline) from the trace recorded in the absence of TTX and a 2-point moving average was employed to smoothen the trace (Figure 6E, Figure S5). A significant increase ($P < 0.0001$, two-tailed unpaired t -test) in fluorescence was observed during the stimulation period with an average $\Delta F/F$ of $0.20 \pm 0.03\%$ (Figure 6F), demonstrating that probe **3** can record voltage changes in axonal projections of dopaminergic neurons in the striatum upon electric stimulation. Notably, the sensitivity of probe **3** to such stimulation is superior (67% higher) to the performance of probe **1** under the same experimental conditions as we showed previously ($\Delta F/F$ of $0.12 \pm 0.03\%$, Figure 6F).⁶² Overall, the combination of a PEG linker with a brighter, azetidinesubstituted dsRVF4 VSD provides a superior sensor which can be selectively delivered to dopaminergic axonal projections in striatal tissue and enables improved recording of membrane potential changes after electric stimulation.

Conclusions

Targeted voltage imaging in brain tissue with chemical probes remains a highly challenging task. An optimal combination of three components should manifest in an ideal sensor: (1) anchoring of the probe to the neurons of interest requires a potent ligand; (2) an efficient carrier molecule is necessary to deliver the highly lipophilic dye to the neurons of interest with minimal background staining; and (3) VSDs with high brightness and sensitivity are required to efficiently report on the changes in membrane potential from the limited, pseudo-2D area of a cell membrane. These requirements are still more important when using endogenously expressed membrane proteins as molecular targets for sensor delivery, due to the relatively small number of delivered dye molecules dictated by the native expression levels of the protein target. This work addresses the latter two components of a targetable voltage sensor. On the delivery vehicle front, we show that for negatively charged PeT-based VSDs, higher targeting selectivity is achieved with PEG compared to dextran as a polymer carrier. On the sensor side, we show that azetidinesubstitution in a rhodol-based VSD substantially increases the brightness of the sensor, translating into higher voltage

sensitivity. With the PEG-supported dsRVF4 VSD, we show a 67% improvement in sensitivity for recording electrically induced activity from dopaminergic axons in mouse striatal slices compared to our previously published dextran-supported dsRVF5 prototype.⁶²

Despite the improved targeting selectivity and voltage sensitivity, averaging of many trials was still necessary to obtain useful signal. Further development on several fronts will be necessary to enable high fidelity, single trial recording of membrane potential changes in defined neuronal populations without the use of genetic manipulation:

(a) *Development of still brighter, more photostable and sensitive VSDs.* Substantial improvements have been achieved on this front recently, enabling single trial voltage recordings in brain tissue with probes targeted to overexpressed genetically introduced anchors.^{60,61} We note that for our system, the detailed membrane action potential dynamics in the striatal dopaminergic axons are unknown and with the DAT-anchored VSD probes we are sampling averaged heterogenous response of a large number of axons over long periods of time (10's of ms) that far exceeds the duration of a single action potential. In other words, our system is not an idealized model system, but a native tissue where the limits of new VSDs and the recording methods can be determined. This work can therefore define the next milestones to be achieved in future research designed to enable single scan 2P recordings under native conditions, *i.e.*, using natively expressed proteins as anchors for VSDs. For 2P microscopy recordings (under standard conditions using a commercially available setup as used in this work), we require an approximately 10-fold improvement in SNR in the brain tissue. This can be achieved either by a 10-fold improvement in VSD sensitivity ($\Delta F/F$) while maintaining the sensor brightness, or a 100-fold increase in the number of collected photons. For example, some electrochromic dyes (*e.g.*, ANNINE dyes) can exhibit a nominal $\Delta F/F$ per 100 mV of over 50% in cultured cells.^{78,79} However, to achieve such a high nominal sensitivity, VSD excitation is carried out only at the very edge of their absorption spectrum, resulting in a low photon budget and highlighting the main limitation of electrochromic dyes. In contrast, the full breadth of absorption and emission spectra of PeT-based VSDs can be utilized. We envision that implementation of the brightness-increasing azetidinesubstitution strategy presented in this work into the recently published rhodamine designs^{60,61} will provide superior PeT-based voltage sensors. Although improved sensors based on combining all state-of-the-art design principles would likely provide substantial improvement of SNR (likely more than 2-fold compared to this work), another several-fold improvement in SNR will have to originate from further advances in the field. Apart from additional improvement in VSD and linker design, superior engineering of photon collection in brain tissue may become a key contributor. We restate that we base these estimates on our slow 2P recordings, which provide deeper tissue imaging possibilities at the cost of slow temporal resolution.

(b) *Imaging hardware and software.* Particularly for 2-photon imaging, minimizing the time spent for movement of the optics and maximizing the photon-collection time is

crucial for high speed and high sensitivity measurements. Further developments in the area of spatial light modulation techniques hold promise here.⁸⁰ Other developments on the engineering front are also contributing to improvements in the field. As an example, modern hybrid detectors can provide substantial improvement in SNR compared to the traditional photomultiplier tubes.

In anticipation of further major developments in the field, both on the front of VSD as well as hardware and software improvement, we believe that our approach to non-genetic targeting of voltage sensors in brain tissue could enable efficient, single-scan action potential recordings in the foreseeable future.

Methods

Preparation and Storage of Stock Solutions. Stock solutions of probes 1–5 were prepared at 500 μ M in DMSO and stored at -80 °C. Stock solutions of APP+ and nomifensine (Sigma-Aldrich, St. Louis, MO) were prepared at 10 mM in DMSO and stored at -80 °C. Stock solutions of tetrodotoxin (TTX; Tocris Bioscience, Bristol, UK) were prepared at 1 mM in distilled water and stored at -20 °C.

Growth of HEK cell culture. A human embryonic kidney 293 (HEK) EM4 cell line stably transfected with human dopamine transporter (hDAT) and an empty-vector transfected EM4 cell line⁷⁴ were provided by Dr. Jonathan Javitch and Dr. Mark Sonders of the Department of Psychiatry at New York State Psychiatric Institute/Columbia University Irving Medical Center. They were cultured in Dulbecco's modified Eagle medium (DMEM) with GlutaMAX (Gibco-Thermo Fisher Scientific, Waltham, MA) supplemented with 10% FBS and 1% Penicillin-Streptomycin.

Determination of IC_{50} of probes 2 and 5 at hDAT via inhibition of APP+ uptake. hDAT-HEK cells (Passage # 15 to 20) were plated at a density of 1.5×10^5 cells/well onto a white, clear-bottom 96-well plate (Greiner Bio-One, Monroe, NC) pre-coated with poly-D-lysine solution (0.1 mg/mL; Alamanda Polymers, Huntsville, AL) and allowed to grow for 24 h to provide around 100% confluency. Prior to the experiment, experimental media [phenol red-free DMEM (Gibco) supplemented with 1% FBS (Atlanta Biologicals, Flowery Branch, GA) and 1% Penicillin-Streptomycin (Invitrogen, Waltham, MA)] was first prepared containing different concentrations of probe 2 or 5 (0.1 nM, 1 nM, 2.15 mM, 4.64 mM, 10 nM, 31.6 nM, 100 nM and 1000 nM) or DMSO (vehicle; same volume as added stock solution of the probe). During the experiment, the cells were washed with DPBS (HyClone, Marlborough, MA; 120 μ L) and pre-incubated with experimental media with the tested compounds or vehicle (63 μ L) for 45 min at 37 °C and in a 5% CO₂ environment. APP+ (1.1 μ M) was then added to all wells and cells were further incubated for 25 min at 37 °C and in a 5% CO₂ environment. After incubation, cells were washed with DPBS (120 μ L) and maintained in DPBS (120 μ L) during the remainder of the APP+ fluorescence uptake measurement, which was performed with a BioTek Synergy Neo2 Hybrid Multi-Mode Reader (Agilent, Santa Clara, CA) using 3 \times 3 area scan and bottom-read mode. The excitation and emission wavelengths were set at 420 nm and 500 nm, respectively. For data analysis, the mean fluorescence of wells containing tested

probes was subtracted from that of the respective wells containing DMSO (vehicle) for each probe concentration. All data were normalized to the maximum fluorescence intensity of a well where APP+ uptake was inhibited by indatraline as a standard DAT blocker at 1 μ M concentration. The IC_{50} of probes 2 and 5 to hDAT was determined by non-linear regression using a 1:1 binding model measuring the dose-dependent inhibition of APP+ uptake ([inhibitor] vs. response – Variable slope; GraphPad Prism version 8, GraphPad Software Inc., San Diego, CA).

Measurement of excitation and fluorescence spectra of fluorescent probes. hDAT-HEK cells (Passage # 15–20) were plated at a density of 1.5×10^5 cells/well onto a white, clear-bottom 96-well plate pre-coated with poly-D-lysine solution (0.1 mg/mL; Alamanda Polymers, Huntsville, AL) and allowed to grow for 24 h to provide around 100% confluency. During the experiment, the cells were washed with DPBS, which was subsequently replaced with experimental media containing the dye solutions at 250 nM concentration and cells were further incubated for 15 min at room temperature. After incubation, cells were washed 2 \times with DPBS and maintained in DPBS during the remainder of the measurement, which was performed with a H1MF plate reader (BioTek, Winooski, VT) at 25 °C using bottom-read mode. Fluorescence emission spectra were measured using an excitation source with $\lambda_{exc} = 530$ nm. Excitation spectra were measured using the emission at $\lambda_{em} = 590$ nm. All spectra were measured with a 1 nm-resolution and normalized.

Cellular brightness and targeting selectivity. *Preparation of HEK cells for imaging.* Cells (passage # 15–20) were plated at a density of 5.0×10^5 or 2.5×10^5 cells/well onto culture-treated 12-well plates (Greiner Bio-One, Monroe, NC) and allowed to grow for 24 h or 48 h, respectively, to provide around 80% confluency for imaging. The growth media were replaced with experimental media containing the probe. The cells were subsequently incubated at 37 °C in a 5% CO₂ environment for 15 min. After incubation, cells were washed 2 \times with DPBS (HyClone) and maintained in DPBS (HyClone) during the course of the imaging experiment.

Imaging HEK cells with one-photon epifluorescence. Imaging was carried out with a Leica DMI4000 epifluorescence microscope (Leica Microsystems, Wetzlar, Germany) equipped with a xenon lamp (Sutter Lambda LS; Sutter Instrument, Novato, CA). Images were obtained with a Leica objective (40 \times /0.45 HI Plan; Leica Microsystems, Wetzlar, Germany) and a PCO.Panda 4.2 camera (PCO, Kelheim, Germany). Filters used include a 540 nm excitation filter (25 nm bandpass), a 570 nm dichroic, and a 605 nm emission filter (55 nm bandpass; all Chroma Technology Corp., Bellows Falls, VT). Images were collected using the Micro-Manager software.⁸¹ Images were resolved in 2048 \times 2048 pixel² in a 225 \times 225 μ m² field of view.

Quantification of probe labeling in HEK cells. Quantification of labeling was done by an experimenter who was blinded to the experimental conditions and expected results. For each experimental condition (hDAT or null), ROIs strictly surrounding individual cell bodies were selected using the “Freehand selections” tool from the brightfield (BF) image without prior knowledge of the respective

epifluorescence (FL) image. Only then were these ROIs applied to the corresponding FL image to measure the mean fluorescence intensity within each ROI (ImageJ, NIH). An ROI was also selected in a cell-free area close to the previously selected cell following the same procedure and the fluorescence intensity of this area was subtracted as background from the corresponding fluorescence intensity of the cell. Each data point (n) represented the average of 5 ROIs. In very rare circumstances, ROIs selected from the BF image included exceedingly uniform bright circular spots in the corresponding FL image, and these ROIs were discarded (these likely represent dead cells). For graphs in Figure 3C, the fluorescence intensity for each probe was normalized to the mean of the respective hDAT-condition (hDAT). For graphs in Figure 3B, the fluorescence intensity for each probe was normalized to the mean of probe 2.

Voltage sensitivity in HEK cells. hDAT-HEK cells were plated on PDL-coated coverslips at a density of $\sim 0.5 \times 10^5$ cells/coverslip. On the day of the experiment, a coverslip was mounted on an upright Olympus BX50WI (Olympus, Tokyo, Japan) microscope equipped with a 40 \times water immersion objective, differential interference contrast (DIC) optics and an infrared video camera and constantly perfused at a rate of 1 mL/min with saline containing (in mM): 118.6 NaCl, 3 KCl, 2.7 HEPES-Na, 3.3 HEPES, 1.2 MgCl₂·6H₂O, 2 CaCl₂, and 10 glucose (pH 7.2 – 7.4, 250 – 255 mOsm/L). Whole-cell recordings were performed with a MultiClamp 700B amplifier (Molecular Devices, Foster City, CA) and InstruTECH ITC-18 A/D board (HEKA, Holliston, MA). Electrophysiological data were acquired using WINWCP software (developed by John Dempster, University of Strathclyde, UK). The pipette solution contained (in mM): 115 K-gluconate, 10 HEPES, 2 MgCl₂, 20 KCl, 2 MgATP, 1 Na₂-ATP, and 0.3 GTP (pH 7.3; 280 \pm 5 mOsm). A cell was held at -60 mV in voltage clamp mode and a series of voltage steps was applied between -100 and +90 mV. Simultaneous recording of VSD optical signal was performed with an ORCA Fusion digital camera (Hamamatsu, Japan) using a DSRed fluorescent filter set (545 nm excitation filter, 30 nm bandpass; 570 nm dichroic; 620 nm emission filter, 60 nm bandpass; Chroma Technology Corp, VT) and recorded using HCLImage software (Hamamatsu, Japan). Electrical and optical signals were synchronized with Master 9 multichannel TTL pulse generator (A.M.P.L., Israel). Background-subtracted time series of images were analyzed in ImageJ (NIH, USA), with the plasma membrane as the ROI.

Preparation of acute murine brain slices. All animal protocols were approved by the Institutional Animal Care and Use Committee of New York State Psychiatric Institute/Columbia University Irving Medical Center. All protocols followed the Guide for the Care and Use of Laboratory Animals by National Institute of Health (NIH). All animals used were C57BL/6, wild-type mice from The Jackson Laboratory (Bar Harbor, ME), included both males and females, and sacrificed between 8 to 10 weeks. Coronal slices (300 μ m thick) were cut by a Leica VT1200 vibratome in ice-cold slicing solution (in mM: 194 sucrose, 30 NaCl, 4.5 KCl, 26 NaHCO₃, 1 MgCl₂·6H₂O, 1.2 NaH₂PO₄, 10 D-Glucose), and transferred to oxygenated (95% O₂ + 5% CO₂), 37 °C artificial cerebrospinal fluid (ACSF, in mM:

124 NaCl, 4.5 KCl, 26 NaHCO₃, 1 MgCl₂·6H₂O, 2 CaCl₂, 1.2 NaH₂PO₄, 10 D-Glucose; pH = 7.30; 295 mOsm) in a slice chamber for 15 min. Slices were then incubated in oxygenated ACSF at room temperature for 30 min before imaging.

Electrical stimulation and two-photon imaging of acute murine brain slices. Slices were transferred to a QE-1 imaging chamber and held in place by a SHD-26H/2 slice anchor (both by Warner Instruments LLC, Hamden, CT). Slices were maintained in a bath of ~ 2 mL, oxygenated ACSF during probe incubation. Slices were perfused with oxygenated ACSF at 2 mL/min during the course of imaging, with tetrodotoxin (TTX; 1 μ M) added to the perfusate only for TTX-treated conditions. Slices were imaged with a Prairie Ultima Multiphoton Microscopy System (Bruker Corp., Billerica, MA), a Ti:sapphire Chameleon Ultra II laser (Coherent Inc., Santa Clara, CA), a Zeiss water-immersion objective (63 \times /0.9 NA; Zeiss, Oberkochen, Germany), and the Prairie View software (version 5.4). Probes were excited at 820 nm and emission collected at 570 – 610 nm. High-resolution images were collected with the galvo scanning mode in the format of 512 \times 512 pixel² or 1024 \times 1024 pixel², 10 μ s/pixel dwell time, and 4 \times optical zoom (55 \times 55 μ m² field of view). To achieve a faster sampling rate (30 frames/second) during the electrical stimulation experiments, images were collected with the spiral scanning mode in the format of 16-bit, 10.4 μ s/pixel dwell time, and 1 \times optical zoom with circular ROIs of 16 pixel in diameter (84 μ m in diameter field of view). Each t-series was imaged for 5 s total, where a single electrically stimulated train was delivered from seconds 2.0 to 2.5 (50 Hz, 25 pulses, each pulse 100 μ s \times 180–200 mA, 0.5 s total) with a bipolar stainless-steel electrode, with each pole of the electrode controlled by an ISO-Flex stimulus isolator triggered by the “Voltage Output” application of the Prairie View software. Here, one of the two isolators were set to be positive and the other negative, and each individual pulse was comprised of a positive pulse immediately followed by a negative pulse (*i.e.*, 100 μ s delay for the negative pulse). For each condition, 100 different ROIs/t-series were taken 25–35 μ m below slice surface with 10 ROIs per slice, 10 total slices across 3 days.

Analysis of electrical stimulation experiments in acute murine brain slices. The total fluorescence of each timeframe of each t-series was plotted as the raw data trace. The normalized raw traces for each condition are shown collectively in Figure S5A, B. Each raw trace was corrected for photobleaching using the two-phase exponential decay function in GraphPad Prism 9. The change in fluorescence ($\Delta F/F$) at each time frame for each bleaching-corrected trace was then calculated. The average of all $\Delta F/F$ traces was shown in Figure S5C. The averaged $\Delta F/F$ trace of the TTX-added condition was subtracted from the $\Delta F/F$ trace of the same condition but with no TTX added and the results shown in Figure S5D. Then a 2-points moving average (of each frame and its previous frame) was applied to each $\Delta F/F$ trace, and for each probe, the average $\Delta F/F$ trace of the TTX-added condition was subtracted from the $\Delta F/F$ trace of the same condition but with no TTX added and the results shown in Figure 6E. Finally, for each probe, the average of all data points from the subtracted

$\Delta F/F$ traces from the pre-stimulation period and those from the stimulation period were shown in Figure 6F with \pm SEM, and the statistical significance analyzed with a two-tailed unpaired t-test using GraphPad Prism 9.

ASSOCIATED CONTENT

Supporting Information. Supplementary figures referenced in the main text, synthetic protocols and NMR spectra. The Supporting Information is available free of charge on the ACS Publications website at <http://pubs.acs.org>.

AUTHOR INFORMATION

Corresponding Authors

***David Sulzer** - Department of Neurology, Psychiatry and Pharmacology, Columbia University Irving Medical Center, New York, NY, USA; Department of Molecular Therapeutics, New York Psychiatric Institute, New York, NY, USA; Email: ds43@cumc.columbia.edu

***Dalibor Sames** - Department of Chemistry, Columbia University, New York, NY, USA; NeuroTechnology Center at Columbia University, New York, NY, USA
orcid.org/0000-0001-6911-2260;
Email: ds584@columbia.edu

Authors

Tomas Fiala - Department of Chemistry, Columbia University, New York, NY, USA; Current address: Laboratory of Organic Chemistry, ETH Zurich, D-CHAB, Vladimir-Prelog-Weg 3, 8093 Zurich, Switzerland;
orcid.org/0000-0001-6949-4561;

Eugene V. Mosharov - Department of Neurology, Columbia University Irving Medical Center, New York, NY, USA;

Jihang Wang - Department of Chemistry, Columbia University, New York, NY, USA;

Adriana M. Mendieta - Department of Chemistry, Columbia University, New York, NY, USA;

Se Joon Choi - Department of Psychiatry, Columbia University Irving Medical Center, New York, NY, USA;

Eva Fialova - Department of Chemistry, Columbia University, New York, NY, USA;

Christopher Hwu - Department of Chemistry, Columbia University, New York, NY, USA;

Notes

The authors declare no competing financial interest.

Author Contributions

T.F. and D. Sames conceptualized the project. T.F., A.M. and E.F. synthesized the probes. T.F., C.H. and A.M. characterized the binding potency of the probes. T.F. and E.F. characterized the targeting and brightness of the probes. E.M. and S.J.C. determined the voltage sensitivity of the probes in cell culture. E.M., S.J.C. and J.W. characterized the targeting specificity of the probes in acute mouse brain slices. J.W. carried out the stimulation experiments in acute mouse brain slices. T.F., E.M., J.W. and E.F. analyzed the data. D. Sames and D. Sulzer oversaw the project. T.F. wrote the paper with important contributions from D. Sames. All authors gave approval to the final version of the manuscript.

ACKNOWLEDGMENTS

We thank Dr. Brandon Fowler (Department of Chemistry, Columbia University) for HRMS analysis. T.F. is the recipient of the Alfred Bader Fellowship in Organic Chemistry. This

work was supported by the G. Harold & Leila Y. Mathers Charitable Foundation (to D. Sames), The National Institute of Mental Health (NIMH) of the National Institutes of Health (NIH), grant R01MH122470 (to D. Sames and D. Sulzer), the National Institute on Drug Abuse (NIDA) of NIH, grant R01DA07418 (to D. Sulzer) and the JPB Foundation (to D. Sulzer).

REFERENCES

- (1) Sakmann, B.; Neher, E. Patch Clamp Techniques for Studying Ionic Channels in Excitable Membranes. *Annu. Rev. Physiol.* **1984**, *46* (1), 455–472. <https://doi.org/10.1146/annurev.ph.46.030184.002323>.
- (2) Segev, A.; Garcia-Oscos, F.; Kourrich, S. Whole-Cell Patch-Clamp Recordings in Brain Slices. *JoVE (Journal of Visualized Experiments)* **2016**, No. 112, e54024. <https://doi.org/10.3791/54024>.
- (3) Sepehri Rad, M.; Choi, Y.; Cohen, L. B.; Baker, B. J.; Zhong, S.; Storace, D. A.; Braubach, O. R. Voltage and Calcium Imaging of Brain Activity. *Biophysical Journal* **2017**, *113* (10), 2160–2167. <https://doi.org/10.1016/j.bpj.2017.09.040>.
- (4) Lavis, L. D. Live and Let Dye. *Biochemistry* **2021**. <https://doi.org/10.1021/acs.biochem.1c00299>.
- (5) Grynkiewicz, G.; Poenie, M.; Tsien, R. Y. A New Generation of Ca²⁺ Indicators with Greatly Improved Fluorescence Properties. *J. Biol. Chem.* **1985**, *260* (6), 3440–3450.
- (6) Stosiek, C.; Garaschuk, O.; Holthoff, K.; Konnerth, A. In Vivo Two-Photon Calcium Imaging of Neuronal Networks. *PNAS* **2003**, *100* (12), 7319–7324. <https://doi.org/10.1073/pnas.1232232100>.
- (7) Kao, J. P. Y.; Li, G.; Auston, D. A. Chapter 5 - Practical Aspects of Measuring Intracellular Calcium Signals with Fluorescent Indicators. In *Methods in Cell Biology*; Whitaker, M., Ed.; Calcium in Living Cells; Academic Press, 2010; Vol. 99, pp 113–152. <https://doi.org/10.1016/B978-0-12-374841-6.00005-0>.
- (8) Zhou, X.; Belavek, K. J.; Miller, E. W. Origins of Ca²⁺ Imaging with Fluorescent Indicators. *Biochemistry* **2021**, *60* (46), 3547–3554. <https://doi.org/10.1021/acs.biochem.1c00350>.
- (9) Vajente, N.; Norante, R.; Pizzo, P.; Pendin, D. Calcium Imaging in Drosophila Melanogaster. In *Calcium Signaling*; Islam, Md. S., Ed.; Advances in Experimental Medicine and Biology; Springer International Publishing: Cham, 2020; pp 881–900. https://doi.org/10.1007/978-3-030-12457-1_35.
- (10) de Melo Reis, R. A.; Freitas, H. R.; de Mello, F. G. Cell Calcium Imaging as a Reliable Method to Study Neuron–Glial Circuits. *Frontiers in Neuroscience* **2020**, *14*, 975. <https://doi.org/10.3389/fnins.2020.569361>.
- (11) Inoue, M. Genetically Encoded Calcium Indicators to Probe Complex Brain Circuit Dynamics in Vivo. *Neuroscience Research* **2021**, *169*, 2–8. <https://doi.org/10.1016/j.neures.2020.05.013>.
- (12) Gubernator, N. G.; Zhang, H.; Staal, R. G. W.; Mosharov, E. V.; Pereira, D. B.; Yue, M.; Balsanek, V.; Vadola, P. A.; Mukherjee, B.; Edwards, R. H.; Sulzer, D.; Sames, D. Fluorescent False Neurotransmitters Visualize Dopamine Release from Individual Presynaptic Terminals. *Science* **2009**, *324* (5933), 1441–1444. <https://doi.org/10.1126/science.1172278>.
- (13) Lee, M.; Gubernator, N. G.; Sulzer, D.; Sames, D. Development of PH-Responsive Fluorescent False Neurotransmitters. *J. Am. Chem. Soc.* **2010**, *132* (26), 8828–8830. <https://doi.org/10.1021/ja101740k>.

- (14) Rodriguez, P. C.; Pereira, D. B.; Borgkvist, A.; Wong, M. Y.; Barnard, C.; Sonders, M. S.; Zhang, H.; Sames, D.; Sulzer, D. Fluorescent Dopamine Tracer Resolves Individual Dopaminergic Synapses and Their Activity in the Brain. *PNAS* **2013**, *110* (3), 870–875. <https://doi.org/10.1073/pnas.1213569110>.
- (15) Pereira, D. B.; Schmitz, Y.; Mészáros, J.; Merchant, P.; Hu, G.; Li, S.; Henke, A.; Lizardi-Ortiz, J. E.; Jr, R. J. K.; Morgenstern, T. J.; Sonders, M. S.; Kanter, E.; Rodriguez, P. C.; Mosharov, E. V.; Sames, D.; Sulzer, D. Fluorescent False Neurotransmitter Reveals Functionally Silent Dopamine Vesicle Clusters in the Striatum. *Nature Neurosci* **2016**, *19* (4), 578–586. <https://doi.org/10.1038/nn.4252>.
- (16) Freyberg, Z.; Sonders, M. S.; Aguilar, J. I.; Hiranita, T.; Karam, C. S.; Flores, J.; Pizzo, A. B.; Zhang, Y.; Farino, Z. J.; Chen, A.; Martin, C. A.; Kopajtic, T. A.; Fei, H.; Hu, G.; Lin, Y.-Y.; Mosharov, E. V.; McCabe, B. D.; Freyberg, R.; Wimalasena, K.; Hsin, L.-W.; Sames, D.; Krantz, D. E.; Katz, J. L.; Sulzer, D.; Javitch, J. A. Mechanisms of Amphetamine Action Illuminated through Optical Monitoring of Dopamine Synaptic Vesicles in *Drosophila* Brain. *Nature Communications* **2016**, *7*, 10652. <https://doi.org/10.1038/ncomms10652>.
- (17) Aguilar, J. I.; Dunn, M.; Mingote, S.; Karam, C. S.; Farino, Z. J.; Sonders, M. S.; Choi, S. J.; Grygoruk, A.; Zhang, Y.; Cela, C.; Choi, B. J.; Flores, J.; Freyberg, R. J.; McCabe, B. D.; Mosharov, E. V.; Krantz, D. E.; Javitch, J. A.; Sulzer, D.; Sames, D.; Rayport, S.; Freyberg, Z. Neuronal Depolarization Drives Increased Dopamine Synaptic Vesicle Loading via VGLUT. *Neuron* **2017**, *95* (5), 1074–1088.e7. <https://doi.org/10.1016/j.neuron.2017.07.038>.
- (18) Dunn, M.; Henke, A.; Clark, S.; Kovalyova, Y.; Kempadoo, K. A.; Karpowicz, R. J.; Kandel, E. R.; Sulzer, D.; Sames, D. Designing a Norepinephrine Optical Tracer for Imaging Individual Noradrenergic Synapses and Their Activity in Vivo. *Nature Communications* **2018**, *9* (1), 2838. <https://doi.org/10.1038/s41467-018-05075-x>.
- (19) Henke, A.; Kovalyova, Y.; Dunn, M.; Dreier, D.; Gubernator, N. G.; Dincheva, I.; Hwu, C.; Šebej, P.; Ansoorge, M. S.; Sulzer, D.; Sames, D. Toward Serotonin Fluorescent False Neurotransmitters: Development of Fluorescent Dual Serotonin and Vesicular Monoamine Transporter Substrates for Visualizing Serotonin Neurons. *ACS Chem Neurosci* **2018**, *9*, 925–934. <https://doi.org/10.1021/acscemneuro.7b00320>.
- (20) Secor, K. E.; Glass, T. E. Selective Amine Recognition: Development of a Chemosensor for Dopamine and Norepinephrine. *Org. Lett.* **2004**, *6* (21), 3727–3730. <https://doi.org/10.1021/ol048625f>.
- (21) Hettie, K. S.; Liu, X.; Gillis, K. D.; Glass, T. E. Selective Catecholamine Recognition with NeuroSensor 521: A Fluorescent Sensor for the Visualization of Norepinephrine in Fixed and Live Cells. *ACS Chem. Neurosci.* **2013**, *4* (6), 918–923. <https://doi.org/10.1021/cn300227m>.
- (22) Hettie, K. S.; Glass, T. E. Turn-On Near-Infrared Fluorescent Sensor for Selectively Imaging Serotonin. *ACS Chem. Neurosci.* **2016**, *7* (1), 21–25. <https://doi.org/10.1021/acscemneuro.5b00235>.
- (23) Feng, P.; Chen, Y.; Zhang, L.; Qian, C.-G.; Xiao, X.; Han, X.; Shen, Q.-D. Near-Infrared Fluorescent Nanoprobes for Revealing the Role of Dopamine in Drug Addiction. *ACS Appl. Mater. Interfaces* **2018**, *10* (5), 4359–4368. <https://doi.org/10.1021/acsami.7b12005>.
- (24) Leopold, A. V.; Shcherbakova, D. M.; Verkhusha, V. V. Fluorescent Biosensors for Neurotransmission and Neuro-modulation: Engineering and Applications. *Front. Cell. Neurosci.* **2019**, *13*. <https://doi.org/10.3389/fncel.2019.00474>.
- (25) Cohen, L. B.; Salzberg, B. M. Optical Measurement of Membrane Potential. In *Reviews of Physiology, Biochemistry and Pharmacology, Volume 83*; Reviews of Physiology, Biochemistry and Pharmacology; Springer, Berlin, Heidelberg, 1978; pp 35–88. https://doi.org/10.1007/3-540-08907-1_2.
- (26) Peterka, D. S.; Takahashi, H.; Yuste, R. Imaging Voltage in Neurons. *Neuron* **2011**, *69* (1), 9–21. <https://doi.org/10.1016/j.neuron.2010.12.010>.
- (27) Loew, L. M. Design and Use of Organic Voltage Sensitive Dyes. In *Membrane Potential Imaging in the Nervous System and Heart*; Advances in Experimental Medicine and Biology; Springer, Cham, 2015; pp 27–53. https://doi.org/10.1007/978-3-319-17641-3_2.
- (28) Miller, E. W. Small Molecule Fluorescent Voltage Indicators for Studying Membrane Potential. *Current Opinion in Chemical Biology* **2016**, *33*, 74–80. <https://doi.org/10.1016/j.cbpa.2016.06.003>.
- (29) Yan, P.; Acker, C. D.; Zhou, W.-L.; Lee, P.; Bollensdorff, C.; Negrean, A.; Lotti, J.; Sacconi, L.; Antic, S. D.; Kohl, P.; Mansvelder, H. D.; Pavone, F. S.; Loew, L. M. Palette of Fluorinated Voltage-Sensitive Hemicyanine Dyes. *Proc Natl Acad Sci U S A* **2012**, *109* (50), 20443–20448. <https://doi.org/10.1073/pnas.1214850109>.
- (30) Reeve, J. E.; Corbett, A. D.; Boczarow, I.; Kaluza, W.; Barford, W.; Bayley, H.; Wilson, T.; Anderson, H. L. Porphyrins for Probing Electrical Potential Across Lipid Bilayer Membranes by Second Harmonic Generation. *Angewandte Chemie International Edition* **2013**, *52* (34), 9044–9048. <https://doi.org/10.1002/anie.201304515>.
- (31) Sayresmith, N. A.; Saminathan, A.; Sailer, J. K.; Patberg, S. M.; Sandor, K.; Krishnan, Y.; Walter, M. G. Photostable Voltage-Sensitive Dyes Based on Simple, Solvatofluorochromic, Asymmetric Thiazolothiazoles. *J. Am. Chem. Soc.* **2019**, *141* (47), 18780–18790. <https://doi.org/10.1021/jacs.9b08959>.
- (32) Rowland, C. E.; Susumu, K.; Stewart, M. H.; Oh, E.; Mäkinen, A. J.; O’Shaughnessy, T. J.; Kushto, G.; Wolak, M. A.; Erickson, J. S.; L. Efros, A.; Huston, A. L.; Delehanty, J. B. Electric Field Modulation of Semiconductor Quantum Dot Photoluminescence: Insights Into the Design of Robust Voltage-Sensitive Cellular Imaging Probes. *Nano Lett.* **2015**, *15* (10), 6848–6854. <https://doi.org/10.1021/acs.nanolett.5b02725>.
- (33) Park, J.; Kuo, Y.; Li, J.; Huang, Y.-L.; Miller, E. W.; Weiss, S. Improved Surface Functionalization and Characterization of Membrane-Targeted Semiconductor Voltage Nanosensors. *J. Phys. Chem. Lett.* **2019**, *10* (14), 3906–3913. <https://doi.org/10.1021/acs.jpcclett.9b01258>.
- (34) Treger, J. S.; Priest, M. F.; Iezzi, R.; Bezanilla, F. Real-Time Imaging of Electrical Signals with an Infrared FDA-Approved Dye. *Biophysical Journal* **2014**, *107* (6), L09-L12. <https://doi.org/10.1016/j.bpj.2014.07.054>.
- (35) Miller, E. W.; Lin, J. Y.; Frady, E. P.; Steinbach, P. A.; Kristan, W. B.; Tsien, R. Y. Optically Monitoring Voltage in Neurons by Photo-Induced Electron Transfer through Molecular Wires. *PNAS* **2012**, *109* (6), 2114–2119. <https://doi.org/10.1073/pnas.1120694109>.
- (36) Woodford, C. R.; Frady, E. P.; Smith, R. S.; Morey, B.; Canzi, G.; Palida, S. F.; Araneda, R. C.; Kristan, W. B.; Kubiak, C. P.; Miller, E. W.; Tsien, R. Y. Improved PeT Molecules for Optically Sensing Voltage in Neurons. *J. Am. Chem. Soc.* **2015**, *137* (5), 1817–1824. <https://doi.org/10.1021/ja510602z>.

- (37) Huang, Y.-L.; Walker, A. S.; Miller, E. W. A Photostable Silicon Rhodamine Platform for Optical Voltage Sensing. *J. Am. Chem. Soc.* **2015**, *137* (33), 10767–10776. <https://doi.org/10.1021/jacs.5b06644>.
- (38) Kulkarni, R. U.; Yin, H.; Pourmandi, N.; James, F.; Adil, M. M.; Schaffer, D. V.; Wang, Y.; Miller, E. W. A Rationally Designed, General Strategy for Membrane Orientation of Photoinduced Electron Transfer-Based Voltage-Sensitive Dyes. *ACS Chem. Biol.* **2017**, *12* (2), 407–413. <https://doi.org/10.1021/acscchembio.6b00981>.
- (39) Kulkarni, R. U.; Kramer, D. J.; Pourmandi, N.; Karbasi, K.; Bateup, H. S.; Miller, E. W. Voltage-Sensitive Rhodol with Enhanced Two-Photon Brightness. *PNAS* **2017**, *114* (11), 2813–2818. <https://doi.org/10.1073/pnas.1610791114>.
- (40) Kulkarni, R. U.; Vandenbergh, M.; Thunemann, M.; James, F.; Andreassen, O. A.; Djurovic, S.; Devor, A.; Miller, E. W. In Vivo Two-Photon Voltage Imaging with Sulfonated Rhodamine Dyes. *ACS Cent. Sci.* **2018**, *4* (10), 1371–1378. <https://doi.org/10.1021/acscentsci.8b00422>.
- (41) Boggess, S. C.; Gandhi, S. S.; Siemons, B. A.; Huebsch, N.; Healy, K. E.; Miller, E. W. New Molecular Scaffolds for Fluorescent Voltage Indicators. *ACS Chem. Biol.* **2019**, *14* (3), 390–396. <https://doi.org/10.1021/acscchembio.8b00978>.
- (42) Franke, J. M.; Raliski, B. K.; Boggess, S. C.; Natesan, D. V.; Koretsky, E. T.; Zhang, P.; Kulkarni, R. U.; Deal, P. E.; Miller, E. W. BODIPY Fluorophores for Membrane Potential Imaging. *J. Am. Chem. Soc.* **2019**, *141* (32), 12824–12831. <https://doi.org/10.1021/jacs.9b05912>.
- (43) Ortiz, G.; Liu, P.; Naing, S. H. H.; Muller, V. R.; Miller, E. W. Synthesis of Sulfonated Carbofluoresceins for Voltage Imaging. *J. Am. Chem. Soc.* **2019**, *141* (16), 6631–6638. <https://doi.org/10.1021/jacs.9b01261>.
- (44) Liu, P.; Miller, E. W. Electrophysiology, Unplugged: Imaging Membrane Potential with Fluorescent Indicators. *Acc. Chem. Res.* **2020**, *53* (1), 11–19. <https://doi.org/10.1021/acs.accounts.9b00514>.
- (45) Gonzalez, M. A.; Walker, A. S.; Cao, K. J.; Lazzari-Dean, J. R.; Settineri, N. S.; Kong, E. J.; Kramer, R. H.; Miller, E. W. Voltage Imaging with a NIR-Absorbing Phosphine Oxide Rhodamine Voltage Reporter. *J. Am. Chem. Soc.* **2021**, *143* (5), 2304–2314. <https://doi.org/10.1021/jacs.0c11382>.
- (46) Xu, Y.; Zou, P.; Cohen, A. E. Voltage Imaging with Genetically Encoded Indicators. *Current Opinion in Chemical Biology* **2017**, *39*, 1–10. <https://doi.org/10.1016/j.cbpa.2017.04.005>.
- (47) Mollinedo-Gajate, I.; Song, C.; Knöpfel, T. Genetically Encoded Voltage Indicators. In *Optogenetics: Light-Sensing Proteins and Their Applications in Neuroscience and Beyond*; Yawo, H., Kandori, H., Koizumi, A., Kageyama, R., Eds.; Advances in Experimental Medicine and Biology; Springer: Singapore, 2021; pp 209–224. https://doi.org/10.1007/978-981-15-8763-4_12.
- (48) Kulkarni, R. U.; Miller, E. W. Voltage Imaging: Pitfalls and Potential. *Biochemistry* **2017**, *56* (39), 5171–5177. <https://doi.org/10.1021/acs.biochem.7b00490>.
- (49) Lavis, L. D. Chemistry Is Dead. Long Live Chemistry! *Biochemistry* **2017**, *56* (39), 5165–5170. <https://doi.org/10.1021/acs.biochem.7b00529>.
- (50) Chanda, B.; Blunck, R.; Faria, L. C.; Schweizer, F. E.; Mody, I.; Bezanilla, F. A Hybrid Approach to Measuring Electrical Activity in Genetically Specified Neurons. *Nature Neuroscience* **2005**, *8* (11), 1619–1626. <https://doi.org/10.1038/nn1558>.
- (51) Ghitani, N.; Bayguinov, P. O.; Ma, Y.; Jackson, M. B. Single-Trial Imaging of Spikes and Synaptic Potentials in Single Neurons in Brain Slices with Genetically Encoded Hybrid Voltage Sensor. *Journal of Neurophysiology* **2015**, *113* (4), 1249–1259. <https://doi.org/10.1152/jn.00691.2014>.
- (52) Abdelfattah, A. S.; Kawashima, T.; Singh, A.; Novak, O.; Liu, H.; Shuai, Y.; Huang, Y.-C.; Campagnola, L.; Seeman, S. C.; Yu, J.; Zheng, J.; Grimm, J. B.; Patel, R.; Friedrich, J.; Mensh, B. D.; Paninski, L.; Macklin, J. J.; Murphy, G. J.; Podgorski, K.; Lin, B.-J.; Chen, T.-W.; Turner, G. C.; Liu, Z.; Koyama, M.; Svoboda, K.; Ahrens, M. B.; Lavis, L. D.; Schreier, E. R. Bright and Photostable Chemigenetic Indicators for Extended in Vivo Voltage Imaging. *Science* **2019**, *365* (6454), 699–704. <https://doi.org/10.1126/science.aav6416>.
- (53) Liu, S.; Lin, C.; Xu, Y.; Luo, H.; Peng, L.; Zeng, X.; Zheng, H.; Chen, P. R.; Zou, P. A Far-Red Hybrid Voltage Indicator Enabled by Bioorthogonal Engineering of Rhodopsin on Live Neurons. *Nat. Chem.* **2021**, *13* (5), 472–479. <https://doi.org/10.1038/s41557-021-00641-1>.
- (54) Hinner, M. J.; Hübener, G.; Fromherz, P. Enzyme-Induced Staining of Biomembranes with Voltage-Sensitive Fluorescent Dyes. *J. Phys. Chem. B* **2004**, *108* (7), 2445–2453. <https://doi.org/10.1021/jp036811h>.
- (55) Hinner, M. J.; Hübener, G.; Fromherz, P. Genetic Targeting of Individual Cells with a Voltage-Sensitive Dye through Enzymatic Activation of Membrane Binding. *ChemBioChem* **2006**, *7* (3), 495–505. <https://doi.org/10.1002/cbic.200500395>.
- (56) Ng, D. N.; Fromherz, P. Genetic Targeting of a Voltage-Sensitive Dye by Enzymatic Activation of Phosphonoxymethyl-Ammonium Derivative. *ACS Chem. Biol.* **2011**, *6* (5), 444–451. <https://doi.org/10.1021/cb100312d>.
- (57) Liu, P.; Grenier, V.; Hong, W.; Muller, V. R.; Miller, E. W. Fluorogenic Targeting of Voltage-Sensitive Dyes to Neurons. *J. Am. Chem. Soc.* **2017**, *139* (48), 17334–17340. <https://doi.org/10.1021/jacs.7b07047>.
- (58) Sundukova, M.; Prifti, E.; Bucci, A.; Kirillova, K.; Serrao, J.; Raymond, L.; Umebayashi, M.; Hovius, R.; Riezman, H.; Johnsson, K.; Heppenstall, P. A. A Chemogenetic Approach for the Optical Monitoring of Voltage in Neurons. *Angewandte Chemie International Edition* **2019**, *58* (8), 2341–2344. <https://doi.org/10.1002/anie.201812967>.
- (59) Grenier, V.; Daws, B. R.; Liu, P.; Miller, E. W. Spying on Neuronal Membrane Potential with Genetically Targetable Voltage Indicators. *J. Am. Chem. Soc.* **2019**, *141* (3), 1349–1358. <https://doi.org/10.1021/jacs.8b11997>.
- (60) Deal, P. E.; Liu, P.; Al-Abdullatif, S. H.; Muller, V. R.; Shamardani, K.; Adesnik, H.; Miller, E. W. Covalently Tethered Rhodamine Voltage Reporters for High Speed Functional Imaging in Brain Tissue. *J. Am. Chem. Soc.* **2020**, *142* (1), 614–622. <https://doi.org/10.1021/jacs.9b12265>.
- (61) Ortiz, G.; Liu, P.; Deal, P. E.; Nensel, A. K.; Martinez, K. N.; Shamardani, K.; Adesnik, H.; Miller, E. W. A Silicon-Rhodamine Chemical-Genetic Hybrid for Far Red Voltage Imaging from Defined Neurons in Brain Slice. *RSC Chem. Biol.* **2021**. <https://doi.org/10.1039/D1CB00156F>.
- (62) Fiala, T.; Wang, J.; Dunn, M.; Šebej, P.; Choi, S. J.; Nwadiabia, E. C.; Fialova, E.; Martinez, D. M.; Cheetham, C. E.; Fogle, K. J.; Palladino, M. J.; Freyberg, Z.; Sulzer, D.; Sames, D. Chemical Targeting of Voltage Sensitive Dyes to Specific Cells and Molecules in the Brain. *J. Am. Chem. Soc.* **2020**, *142* (20), 9285–9301. <https://doi.org/10.1021/jacs.0c00861>.

- (63) Meltzer, P. C.; Liang, A. Y.; Brownell, A. L.; Elmaleh, D. R.; Madras, B. K. Substituted 3-Phenyltropane Analogs of Cocaine: Synthesis, Inhibition of Binding at Cocaine Recognition Sites, and Positron Emission Tomography Imaging. *J. Med. Chem.* **1993**, *36* (7), 855–862. <https://doi.org/10.1021/jm00059a010>.
- (64) Carroll, F. I.; Mascarella, S. W.; Kuzemko, M. A.; Gao, Y.; Abraham, P.; Lewin, A. H.; Boja, J. W.; Kuhar, M. J. Synthesis, Ligand Binding, and QSAR (CoMFA and Classical) Study of 3.Beta.-(3'-Substituted Phenyl)-, 3.Beta.-(4'-Substituted Phenyl)-, and 3.Beta.-(3',4'-Disubstituted Phenyl)Tropane-2.Beta.-Carboxylic Acid Methyl Esters. *J. Med. Chem.* **1994**, *37* (18), 2865–2873. <https://doi.org/10.1021/jm00044a007>.
- (65) Prifti, E.; Reymond, L.; Umebayashi, M.; Hovius, R.; Riezman, H.; Johnsson, K. A Fluorogenic Probe for SNAP-Tagged Plasma Membrane Proteins Based on the Solvatochromic Molecule Nile Red. *ACS Chem. Biol.* **2014**, *9* (3), 606–612. <https://doi.org/10.1021/cb400819c>.
- (66) Shields, B. C.; Kahuno, E.; Kim, C.; Apostolides, P. F.; Brown, J.; Lindo, S.; Mensh, B. D.; Dudman, J. T.; Lavis, L. D.; Tadross, M. R. Deconstructing Behavioral Neuropharmacology with Cellular Specificity. *Science* **2017**, *356* (6333), eaaj2161. <https://doi.org/10.1126/science.aaj2161>.
- (67) Wu, T.; Chen, K.; He, S.; Liu, X.; Zheng, X.; Jiang, Z.-X. Drug Development through Modification of Small Molecular Drugs with Monodisperse Poly(Ethylene Glycol)s. *Org. Process Res. Dev.* **2020**, *24* (8), 1364–1372. <https://doi.org/10.1021/acs.oprd.0c00273>.
- (68) Yadav, D.; Dewangan, H. K. PEGYLATION: An Important Approach for Novel Drug Delivery System. *Journal of Biomaterials Science, Polymer Edition* **2021**, *32* (2), 266–280. <https://doi.org/10.1080/09205063.2020.1825304>.
- (69) Grigoletto, A.; Tedeschini, T.; Canato, E.; Pasut, G. The Evolution of Polymer Conjugation and Drug Targeting for the Delivery of Proteins and Bioactive Molecules. *WIREs Nanomedicine and Nanobiotechnology* **2021**, *13* (3), e1689. <https://doi.org/10.1002/wnan.1689>.
- (70) Liu, Y.; Yang, Y.; Zhang, Q.; Lu, D.; Li, S.; Li, J.; Yang, G.; Shan, Y. Dynamics of Delivering Aptamer Targeted Nano-Drugs into Cells. *Journal of Materials Chemistry B* **2021**, *9* (4), 952–957. <https://doi.org/10.1039/D0TB02527E>.
- (71) Wu, J.; Zhao, C.; Lin, W.; Hu, R.; Wang, Q.; Chen, H.; Li, L.; Chen, S.; Zheng, J. Binding Characteristics between Polyethylene Glycol (PEG) and Proteins in Aqueous Solution. *J. Mater. Chem. B* **2014**, *2* (20), 2983–2992. <https://doi.org/10.1039/C4TB00253A>.
- (72) Wang, K. H.; Penmatsa, A.; Gouaux, E. Neurotransmitter and Psychostimulant Recognition by the Dopamine Transporter. *Nature* **2015**, *521* (7552), 322–327. <https://doi.org/10.1038/nature14431>.
- (73) Grimm, J. B.; English, B. P.; Chen, J.; Slaughter, J. P.; Zhang, Z.; Revyakin, A.; Patel, R.; Macklin, J. J.; Normanno, D.; Singer, R. H.; Lionnet, T.; Lavis, L. D. A General Method to Improve Fluorophores for Live-Cell and Single-Molecule Microscopy. *Nature Methods* **2015**, *12* (3), 244–250. <https://doi.org/10.1038/nmeth.3256>.
- (74) Karpowicz, R. J.; Dunn, M.; Sulzer, D.; Sames, D. APP+, a Fluorescent Analogue of the Neurotoxin MPP+, Is a Marker of Catecholamine Neurons in Brain Tissue, but Not a Fluorescent False Neurotransmitter. *ACS Chem. Neurosci.* **2013**, *4* (5), 858–869. <https://doi.org/10.1021/cn400038u>.
- (75) Kozak, D.; Chen, A.; Bax, J.; Trau, M. Protein Resistance of Dextran and Dextran-Poly(Ethylene Glycol) Copolymer Films. *Biofouling* **2011**, *27* (5), 497–503. <https://doi.org/10.1080/08927014.2011.584618>.
- (76) Lein, E. S.; Hawrylycz, M. J.; Ao, N.; Ayres, M.; Bensinger, A.; Bernard, A.; Boe, A. F.; Boguski, M. S.; Brockway, K. S.; Byrnes, E. J.; Chen, L.; Chen, L.; Chen, T.-M.; Chin, M. C.; Chong, J.; Crook, B. E.; Czaplinska, A.; Dang, C. N.; Datta, S.; Dee, N. R.; Desaki, A. L.; Desta, T.; Diep, E.; Dolbeare, T. A.; Donelan, M. J.; Dong, H.-W.; Dougherty, J. G.; Duncan, B. J.; Ebbert, A. J.; Eichele, G.; Estin, L. K.; Faber, C.; Facer, B. A.; Fields, R.; Fischer, S. R.; Fliss, T. P.; Frensley, C.; Gates, S. N.; Glattfelder, K. J.; Halverson, K. R.; Hart, M. R.; Hohmann, J. G.; Howell, M. P.; Jeung, D. P.; Johnson, R. H.; Karr, P. T.; Kawal, R.; Kidney, J. M.; Knapik, R. H.; Kuan, C. L.; Lake, J. H.; Laramie, A. R.; Larsen, K. D.; Lau, C.; Lemon, T. A.; Liang, A. J.; Liu, Y.; Luong, L. T.; Michaels, J.; Morgan, J. J.; Morgan, R. J.; Mortrud, M. T.; Mosqueda, N. F.; Ng, L. L.; Ng, R.; Orta, G. J.; Overly, C. C.; Pak, T. H.; Parry, S. E.; Pathak, S. D.; Pearson, O. C.; Puchalski, R. B.; Riley, Z. L.; Rockett, H. R.; Rowland, S. A.; Royall, J. J.; Ruiz, M. J.; Sarno, N. R.; Schaffnit, K.; Shapovalova, N. V.; Sivisay, T.; Slaughterbeck, C. R.; Smith, S. C.; Smith, K. A.; Smith, B. I.; Sood, A. J.; Stewart, N. N.; Stumpf, K.-R.; Sunkin, S. M.; Sutram, M.; Tam, A.; Teemer, C. D.; Thaller, C.; Thompson, C. L.; Varnam, L. R.; Visel, A.; Whitlock, R. M.; Wohnoutka, P. E.; Wolkey, C. K.; Wong, V. Y.; Wood, M.; Yaylaoglu, M. B.; Young, R. C.; Youngstrom, B. L.; Yuan, X. F.; Zhang, B.; Zwingman, T. A.; Jones, A. R. Genome-Wide Atlas of Gene Expression in the Adult Mouse Brain. *Nature* **2007**, *445* (7124), 168–176. <https://doi.org/10.1038/nature05453>.
- (77) Interactive Atlas Viewer :: Atlas Viewer <http://atlas.brainmap.org/atlas?atlas=2#atlas=2&plate=100884129&structure=549&x=7799.908447265625&y=4023.3484268188477&z=5> (accessed 2018 -08 -07).
- (78) Fromherz, P.; Hübener, G.; Kuhn, B.; Hinner, M. J. ANNINE-6plus, a Voltage-Sensitive Dye with Good Solubility, Strong Membrane Binding and High Sensitivity. *Eur Biophys J* **2008**, *37* (4), 509–514. <https://doi.org/10.1007/s00249-007-0210-y>.
- (79) Kuhn, B.; Roome, C. J. Primer to Voltage Imaging With ANNINE Dyes and Two-Photon Microscopy. *Frontiers in Cellular Neuroscience* **2019**, *13*, 321. <https://doi.org/10.3389/fncel.2019.00321>.
- (80) Carrillo-Reid, L.; Yang, W.; Kang Miller, J.; Peterka, D. S.; Yuste, R. Imaging and Optically Manipulating Neuronal Ensembles. *Annual Review of Biophysics* **2017**, *46* (1), 271–293. <https://doi.org/10.1146/annurev-biophys-070816-033647>.
- (81) Edelstein, A.; Amodaj, N.; Hoover, K.; Vale, R.; Stuurman, N. Computer Control of Microscopes Using MManager. *Current Protocols in Molecular Biology* **2010**, *92* (1), 14.20.1–14.20.17. <https://doi.org/10.1002/0471142727.mb1420s92>.

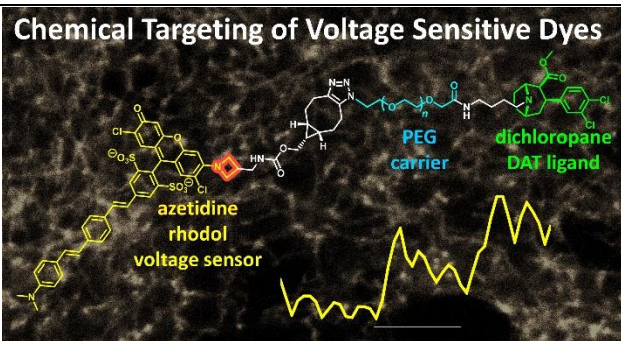


Table of Contents Artwork